Journal of Applied Mechanics and Technical Physics, Vol. 50, No. 5, pp. 891–900, 2009

MODELING COMPLEX PLASTIC DEFORMATION AND FRACTURE OF METALS UNDER DISPROPORTIONATE LOADING

I. A. Volkov. Yu. G. Korotkikh, and I. S. Tarasov

UDC 539.3

A mathematical model is developed to describe fatigue-damage accumulation in structural materials (metals and their alloys) on multiaxial paths of disproportionate combined heat and power loading. The effect of the shape of the strain path on the fatigue life of metals was studied to obtain qualitative and quantitative estimates of the obtained constitutive relations. It is shown that the proposed constitutive relations adequately describe the main elastoplastic deformation effects and damage accumulation in structural materials for arbitrary strain paths.

Key words: *stress–strain state, plasticity, damage, fracture, complex loading, low-cycle fatigue, endurance, life.*

Introduction. During long-term operation of equipment and systems of important engineering facilities under nonstationary heat and power loading, fatigue damage is accumulated in structural materials, leading to deterioration of the initial strength characteristics of the materials and development of defects. During a significant period of operation, these processes occur latently. In addition, the most dangerous zones determining the life of an element are as a rule inaccessible for nondestructive inspection. To ensure safe operation of engineering facilities, it is necessary to monitor damage development in the most dangerous zones of structural elements (exhausted life) and predict the development of these processes to the limiting states (residual life) [1].

Simultaneous studies of deformation and fracture processes provides answer to the following questions: Where and when will macroscopic cracks arise for the first time in a body under specified load and temperature variations and how will these cracks further develop? Because damage accumulation depends significantly on the kinetics of the stress–strain state, the accuracy of estimation of the strength and life of structural elements depends on how precisely the equations of state describe kinetics under specified operation conditions. Viscoelastic deformation parameters such as the length and shape of the strain path, stress mode, its history, etc. have a significant effect on the rate of damage accumulation. The purpose of studies in this area is not so much to refine the various formulations required to determine macroscopic strains from specified loading history, but rather to study the main regularities of the determining and preceding processes.

1. Constitutive Relations of Fracture Mechanics and Algorithm for Their Integration. The model for a damaged medium includes three components: a) relations determining the elastoplastic behavior of the material and dependent on the fracture process; b) equations describing the damage accumulation kinetics; c) strength criterion of the damaged material.

1.1. *Thermal Plasticity Relations.* The constitutive relations of thermal plasticity are based on the following main principles:

— The strain tensors e_{ij} and strain rates tensors $\dot{e}_{ij}$ are the sums of the elastic strains e^e_{ij} and elastic strain rates $\dot{e}^e_{ij}$ (independent of the loading history and determined by the final state of the process), and the plastic strains e^p_{ij} and the plastic strain rates $\dot{e}^p_{ij}$ (dependent on the loading history);

Volga State Academy of Water Transport, Nizhny Novgorod, 603000: schuran@yandex.ru. Translated from Prikladnaya Mekhanika i Tekhnicheskaya Fizika, Vol. 50, No. 5, pp. 193–205, September–October, 2009. Original article submitted November 7, 2007; revision submitted August 26, 2008.

— At various temperatures, the initial yield surface is described by the Mises surface, and the evolution of the yield surface is described by the variation of its radius C_p and the displacement of its center ρ_{ij};
— The principle of gradientality of the plastic strain rate vector to the yield surface at the loading point is valid;
— The body volume varies according to the elastic law;
— Media which are isotropic in the initial state are considered;
— Only the anisotropy due to plastic deformation is considered.

In formulating the constitutive relations stress, we expand the stress σ_{ij} and strain tensors e_{ij} and their increments into the spherical components σ, $\Delta\sigma$, e, and Δe and deviator components σ'_{ij}, $\Delta\sigma'_{ij}$, and e'_{ij}, and $\Delta e'_{ij}$:

$$\sigma_{ij} = \sigma'_{ij} + \sigma\delta_{ij}, \qquad \Delta\sigma_{ij} = \Delta\sigma'_{ij} + \Delta\sigma\delta_{ij}, \qquad \sigma = \sigma_{ii}/3,$$

$$e_{ij} = e'_{ij} + e\delta_{ij}, \qquad \Delta e_{ij} = \Delta e'_{ij} + \Delta e\delta_{ij}, \qquad e = e_{ii}/3$$

(δ_{ij} is the Kronecker tensor).

In the elastic region, the relationship between the spherical and deviator components of the stress and strain tensors is given by Hook's law

$$\begin{gathered} \sigma = 3K[e - \alpha(T - T_0)], \qquad \sigma'_{ij} = 2G(e^e_{ij})', \\ \Delta\sigma = 3K[\Delta e - \Delta(\alpha T)] + \frac{\Delta K}{K}\,\sigma, \qquad \Delta\sigma'_{ij} = 2G\Delta(e^e_{ij})' + \frac{\Delta G}{G}\,\sigma'_{ij}, \end{gathered} \tag{1}$$

where T is the temperature, T_0 is the initial temperature, $K(T)$ is the bulk compression modulus, $G(T)$ is the shear modulus, and $\alpha(T)$ is linear temperature-expansion coefficient of the material.

The effects of monotonic and cyclic deformation in the stress space are described by introducing the yield surface given by the equation

$$F_s = S_{ij}S_{ij} - C_p^2 = 0, \qquad S_{ij} = \sigma'_{ij} - \rho_{ij}. \tag{2}$$

The complex cyclic deformation modes in the stress space is described by introducing the cyclic memory surface. The memory surface which allows monotonic deformation processes to be separated from cyclic processes is given by the equation

$$F_\rho = \rho_{ij}\rho_{ij} - \rho^2_{\max} = 0, \tag{3}$$

where $\rho_{\max}$ is the value of the modulus ρ_{ij} which is maximal throughout the loading history.

We assume that the evolutionary equation for the radius of the yield surface has the following structure [2]:

$$\dot C_p = [q_\chi H(F_\rho) + a(Q_s - C_p)\Gamma(F_\rho)]\dot\chi + q_3\dot T; \tag{4}$$

$$C_p = C_p^0 + \int\limits_t^0 C_p^0, \qquad \dot\chi = \Big(\frac{2}{3}\,\dot e^p_{ij}\dot e^p_{ij}\Big)^{1/2}, \qquad \chi_m = \int\limits_0^t \dot\chi H(F_\rho)\,dt, \qquad \chi = \int\limits_0^t \dot\chi\,dt; \tag{5}$$

$$q_\chi = \frac{q_2 A\psi_1 + (1-A)q_1}{A\psi_1 + 1 - A}, \qquad Q_s = \frac{Q_2 A\psi_2 + (1-A)Q_1}{A\psi_2 + 1 - A}, \qquad 0 \leqslant \psi_i \leqslant 1, \quad i = 1, 2,$$

$$A = 1 - \cos^2\theta, \quad \cos\theta = n^e_{ij}n^s_{ij}, \quad n^e_{ij} = \dot e'_{ij}/(\dot e'_{ij}\dot e'_{ij})^{1/2}, \quad n^s_{ij} = S_{ij}/(S_{ij}S_{ij})^{1/2}, \tag{6}$$

$$H(F_\rho) = \begin{cases} 1, & F_\rho = 0 \wedge \rho_{ij}\dot\rho_{ij} > 0, \\ 0, & F_\rho < 0 \vee \rho_{ij}\dot\rho_{ij} \leqslant 0, \end{cases} \qquad \Gamma(F_\rho) = 1 - H(F_\rho).$$

Here q_1, q_2, and q_3 are the isotropic hardening moduli, Q_1 and Q_2 are the cyclic isotropic hardening moduli, a is a constant that determines the rate of establishment of the cyclic strain hysteresis loop, Q_s is the stationary value of the radius of the yield surface for given $\rho_{\max}$ and T, and C_p^0 is the initial radius of the yield surface.

In Eq. (4), the first term describes the isotropic hardening due to monotonic plastic deformation ($H(F_\rho) = 1$ and $\Gamma(F_\rho) = 0$), the second term describes the cyclic hardening of the material [$H(F_\rho) = 0$ and $\Gamma(F_\rho) = 1$], and the third term describes the variation in the radius of the yield surface with temperature variation.

The isotropic hardening modulus q_χ takes into account the variation in the isotropic hardening of the material as a function of the strain direction at a given point of the path — the angle θ between the strain deviator increment vector which has directing cosines n^e_{ij} and the normal to the yield surface determined by the directing cosines n^s_{ij}. For proportional loading, $\theta = 0$, $A = 0$, and $q_\chi = q_1$ [q_1 is the isotropic hardening modulus of the material under proportional loading (uniaxial tension of the sample)]. For disproportionate loading, we have $\theta = \pi/2$, $A = 1$, and $q_\chi = q_2$ [q_2 is the hardening modulus for loading along the tangent to the yield surface (neutral loading)].

In the case of cyclic isotropic hardening for cyclic proportional loading [see Eq. (4)], we have $\theta = 0$ and $Q_s = Q_1$, and for cyclic disproportionate loading, we have $\theta = \pi/2$ and $Q_s = Q_2$. The calibration (weight) coefficients ψ_1 and ψ_2 are parameters that allow a correction of the effect of the moduli q_1, q_2, Q_1, and Q_2 on the isotropic hardening of the material.

During stationary cyclic deformation with constant strain amplitude and temperature T ($\rho_{\max} = \text{const}$ and $Q_s = \text{const}$), the radius of the yield surface C_p tends to a value $Q_s = \text{const}$ and the hysteresis loop tends to the stationary value determined by the value of Q_s dependent on the current values of T and $\rho_{\max}$.

The equation for the displacement of the yield surface is based on Il'yushin hypothesis assuming that the hardening depends on the deformation history only at a certain nearest site of the path (lag of vector properties). For the internal variable ρ_{ij} describing the hardening anisotropy of plastic deformation, the evolutionary equation is written in the following form [2]

$$\dot\rho_{ij} = g_1 \dot e^p_{ij} - g_2 \rho_{ij} \dot\chi - g_3 \rho_{ij} \dot T, \qquad \rho_{ij} = \int\limits_0^t \dot\rho_{ij}\, dt, \tag{7}$$

where $g_1 > 0$, $g_2 > 0$, and $g_3 > 0$ are the anisotropic hardening moduli.

To describe the evolution of the memory surface, it is necessary of formulate the evolutionary equation for $\rho_{\max}$:

$$\dot\rho_{\max} = \frac{(\rho_{ij}\dot\rho_{ij}) H(F_\rho)}{(\rho_{mn}\rho_{mn})^{1/2}} - g_2 \rho_{\max} \dot\chi - g_3 \rho_{\max} \dot T. \tag{8}$$

In (8), the second the term describes the decay of the memory of the previous cyclic deformation of the material.

Relations (3) and (6) allow an automatic separation of cyclic loading from monotonic loading by means of the operators $H(F_\rho)$ and $\Gamma(F_\rho)$.

The plastic strain rate tensor components are determined from the law of gradientality of the plastic strain rate vector to the yield surface at the loading point:

$$\dot e^p_{ij} = \lambda S_{ij}. \tag{9}$$

Here λ is the proportionality coefficient determined from the condition that, at the end of loading, the new yield surface passes through the end of the stress deviator vector.

The material parameters q_1, q_3, g_1, g_2, and g_3 are determined from the results of tests of cylindrical tubular samples under special cyclic programs of uniaxial tension–compression [2].

The value of Q_1 is determined in tests of samples under block cyclic symmetric loading with specified strain amplitude in each block before stabilization of the hysteresis loop for each value of the strain amplitude. The parameter a in (4) is determined so as to provide the best approximation of experimental laws as C_p tends to a steady state.

To determine q_2 in (4), it is necessary to perform an experiment with complex loading: tension to a certain value $(e^p_{11})^*$ with subsequent torsion to construct the stress path in the space $\sigma_{11} \sim \sigma_{12}$.

To determine Q_2 in (4), it is necessary to perform an experiment with two-block cyclic deformation with the same specified strain amplitude in each block. The first block involves symmetric cyclic loading (tension–compression) up to the establishment of a hysteresis loop, and the second block involves the subsequent cyclic symmetric loading of the sample (torsion) up to the stabilization of the hysteresis loop.

1.2. *Evolutionary Equations of Damage Accumulation.* In the formulation of models for damage accumulation taking into account fatigue mechanisms, the following main principles [2] are used:

— the main stages of the fracture process are modeled;

— for each deformation mechanism, an adequate internal time is introduced to measure the physical life of material;

— nonlinear summation of damage with variation in loading conditions is taken into account;

— damage accumulation processes for various loading conditions and various stress–strain states are equivalent;
— allowance is made for the effect of the strain path shape and stress–strain parameters on the damage accumulation rate;
— allowance is made for the real loading history and the effect of loading history on the damage accumulation rate.

The evolutionary equation of fatigue damage accumulation has the following structure [2]:

$$\dot{\omega} = \frac{\alpha_p + 1}{r_p + 1} f_p(\beta) Z_p^{\alpha_p} (1 - \dot{\omega}_p)^{-r_p} \langle \dot{Z}_p \rangle + \frac{\alpha_e + 1}{r_e + 1} f_e(\beta) Z_e^{\alpha_e} (1 - \dot{\omega}_e)^{-r_e} \langle \dot{Z}_e \rangle; \tag{10}$$

$$Z_p = \frac{W_p - W_a}{W_p^f - W_a}, \qquad Z_e = \frac{W_e - W_b}{W_e^f}; \tag{11}$$

$$\langle \dot{Z} \rangle = \begin{cases} \dot{Z}, & \dot{Z} > 0, \\ 0, & \dot{Z} \leqslant 0, \end{cases} \qquad \langle \dot{Z}_p \rangle = \frac{\langle \dot{W}_p \rangle}{W_p^f - W_a}, \qquad \langle \dot{Z}_e \rangle = \frac{\dot{W}_e}{W_e^f}; \tag{12}$$

$$\dot{W}_p = \rho_{ij}^p \dot{e}_{ij}^p, \qquad \dot{W}_e = \sigma'_{ij} \dot{e}'^e_{ij}. \tag{13}$$

Here α_p, α_e, r_p, and r_e are material parameters which depend on the temperature T, $f(\beta)$ is a function of the three-dimensionality parameter of the stress state $\beta = \sigma/\sigma_u$ [$\sigma_u = (\sigma'_{ij}\sigma'_{ij})^{1/2}$ is the stress intensity], $\dot{W}_p = \int\limits_0^t \dot{W}_p \, dt$a and $\dot{W}_e = \int\limits_0^t \dot{W}_e \, dt$ are the energies expended in the formation of diffuse fatigue damage for low-cycle and multicycle fatigue, respectively, and W_a and W_b are the values of W_p at the end of nucleation of microdefects for low-cycle and multicycle fatigue, respectively.

Integration of Eq. (11) along the strain path yields

$$\omega = 1 - [1 - (y_p^{\alpha_p + 1} + y_e^{\alpha_e + 1})]^{1/(r+1)}, \qquad y_p = A_p Z_p, \qquad y_e = A_e Z_e; \tag{14}$$

$$A_p = \Big[\frac{\alpha_p + 1}{Z_p^{\alpha_p + 1}} \int\limits_0^{Z_p} f_p(\beta) Z_p^{\alpha_p} \, \langle dZ_p \rangle \Big]^{1/(\alpha_p + 1)}; \tag{15}$$

$$A_e = \Big[\frac{\alpha_e + 1}{Z_e^{\alpha_e + 1}} \int\limits_0^{Z_e} f_e(\beta) Z_e^{\alpha_e} \, \langle dZ_e \rangle \Big]^{1/(\alpha_e + 1)}. \tag{16}$$

Equation (14) describes the unified curve of fatigue damage accumulation obtained in symmetric tension–compression tests of laboratory samples. The quantities y_p and y_e are generalized power parameters which are the internal times of the given processes which is used to measure the operation time of the material in the dangerous zone under fatigue (if necessary, the internal time can be converted to the number of characteristic loading cycles commonly used by engineers).

Experimental determination of the material parameters of the evolutionary equations of damage accumulation is performed in the second stage of the process, in which damage begins to influence the physicomechanical characteristics of the material, along with calculation of experimental deformation processes using the constitutive relations of fracture mechanics. All deviations of the results of numerical simulation of deformation ignoring damage from experimental data obtained in the second stage of the damage accumulation process are attributed to the effect of ω (a decrease in the elastic moduli, an increase in the strain amplitude at a constant stress amplitude, a decrease in the stress amplitude at a constant strain amplitude, etc.) [2].

The boundaries W_a and W_b can be determined approximately from the time of onset of softening (increase in strain amplitude or decrease in stress amplitude, respectively) [2] using fatigue test results for a given stress or strain amplitude.

The variation of ω can be established from the variation of the stress amplitude for a given plastic strain amplitude. Integration of the constitutive equation (10) for uniaxial tension–compression yields relations which are the basic relations for determining $\alpha_i = \alpha_i(T)$ and $r_i = r_i(T)$ $(i \equiv e, p)$ [2].

To determine the parameters of the function $f(\beta)$, it is necessary to perform experiments for various values of $\beta_i = \text{const}$. Because, at present, there are no experimental data to determine these parameters, it is possible to use the assumption that, for pure shear $f(\beta) = 1$ for $\beta = 0$; $f(\beta) \to 0$ for $\beta \to -\infty$, and $f(\beta) \to +\infty$ for $\beta \to +\infty$. For uniaxial tension–compression, the work required to form a macroscopic crack is approximately 1.5–2 times greater than the work for pure shear [1, 2].

1.3. *Strength Criterion for Damaged Material.* The criteria for the termination of the phase of development of diffuse microdamage (stage of macrocrack formation) is taken to be instability of damage accumulation processes when the derivatives $\partial\omega_e/\partial y_e$ or $\partial\omega_p/\partial y_p$ reach critical values:

$$\frac{\partial\omega_p}{\partial y_p} = \Big(\frac{\partial\omega_p}{\partial y_p}\Big)_f, \qquad \frac{\partial\omega_e}{\partial y_e} = \Big(\frac{\partial\omega_e}{\partial y_e}\Big)_f. \tag{17}$$

After conditions (17) are satisfied, the further development of the damage processes depends on various random factors and these processes are therefore cannot be controlled. Numerical studies have shown that conditions (17) correspond to the value

$$\omega = \omega_f \simeq 0.8. \tag{18}$$

The main characteristics of elastoplastic deformation (state variables), which are generally described by the tensors σ_{ij}, e_{ij}, e^p_{ij}, and ρ_{ij} and the scalars χ, C_p, ω, and T, can be determined by two methods [3, 4].

The first method involves integration of the constitutive relations with respect to time using any method for solving the Cauchy problem [3].

The second method, with the corresponding formulation of the constitutive relations and linearization of the algorithm of determining λ reduces to writing the thermal plasticity equations in increments which depend on the chosen step Δt. The time step Δt can be corrected in complex regions of the strain path (for example, a break of the path) or can be set constant throughout the calculation provided stability of the calculations. This approach [4], which is the most convenient for boundary-value problems of deformable solid mechanics, is used in the present work.

2. Comparison of Numerical Results with Experimental Data. To justify and verify the physical reliability of the constitutive plasticity relations, it is necessary to perform experiments with the maximally wide range of path curvature in the same experiment. Of special interest are experimental studies of complex unloading of materials and variation of their scalar and vector characteristics. Thus, experiments with complex active loading and unloading of materials on planar curvilinear and spatial polygonal broken paths, as well as numerical analysis of these processes, are very important [5–7].

Experimental results on the stress–strain state of a cylindrical shell in torsional tension in the strain space (rigid loading) on a four-link polygonal path (Fig. 1) are presented in [7]. (In Fig. 1–4, arrows show the direction of motion along the path.) The experiments were performed with a steel tubular specimen with wall thickness $h = 1$ mm, midsurface radius $R = 15.5$ mm, and test-section length $l = 110$ mm.

A feature of the program was that simple torsional strain to the point A (see Fig. 1) was followed by a break of the strain path, after which complex unloading of the sample occurred. (After the break of the path A, the sample was subjected to simultaneous torsion and tension along the path from the point A to the point B. In this case, the sample was unloaded in torsion with simultaneous increase in the tension strain.) After the second break of the path at the point B, the sample was unloaded in compression at a constant value of the torsional strain along the path to the point C. After the third 90° break of the strain path at the point C, the sample was again twisted along the path to the point D. In numerical modeling of experimental data using the constitutive relations, the experimental strain paths [variation of the strain tensor components $e_{ij}(t)$] were specified, and stress paths were obtained by integration of the constitutive relations (1)–(9) on the specified path e_{ij}. The numerical results were compared with experimental data. The calculations were performed for the following parameters of the material [7]: shear modulus $G = 76{,}923$ MPa, bulk compression modulus $K = 166{,}667$ MPa, initial radius of the yield surface $C_p^0 = 370$ MPa, and anisotropic hardening moduli $g_1 = 8000$ MPa and $g_2 = 20$.

Figure 2 gives the calculated stress path which corresponds to the experimental strain path.

Figure 3 presents local strain diagrams (dependences of $\sigma_{11} \sim e_{11}$ and $\sigma_{12} \sim e_{12}$), and Fig. 4 presents a complex-strain diagram (curve of the stress tensor intensity versus the strain tensor intensity $\sigma_u \sim e_u$). It is evident from Figs. 2–4, that the numerical results and experimental data [7] are in good agreement (the points A', B', C',

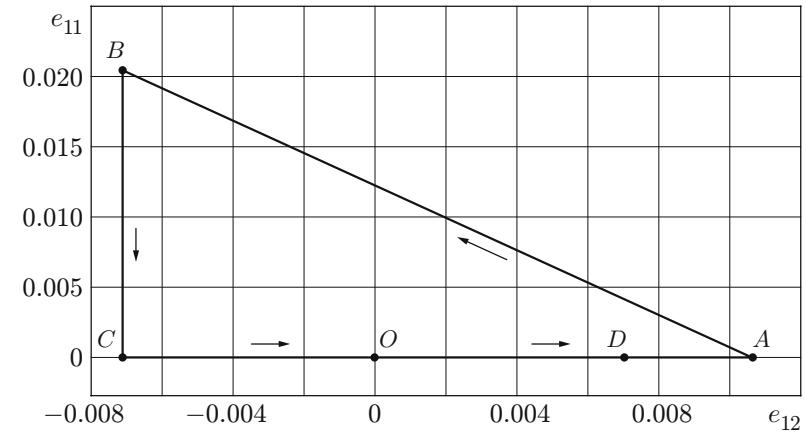

Fig. 1. Experimental path of complex plastic deformation (torsional tension) [7].

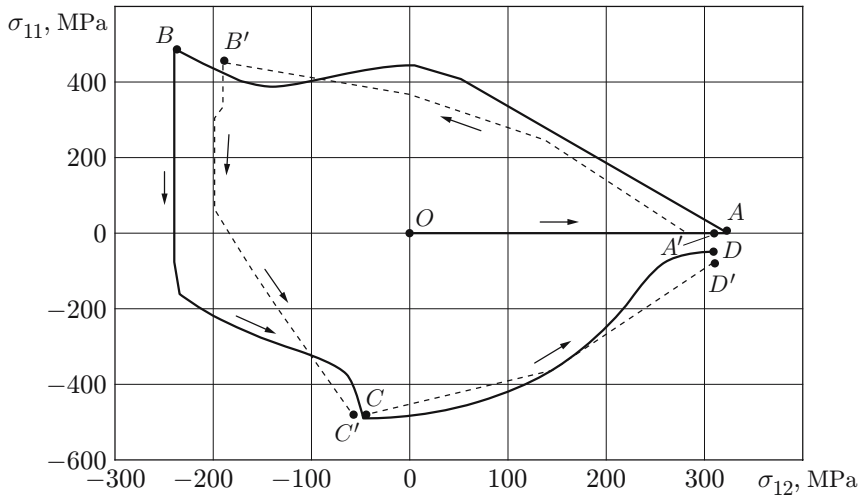

Fig. 2. Calculated stress path corresponding to the experimental strain paths: the solid curve corresponds to numerical results, and the dashed curve to experimental data [7].

and D' show the calculated values corresponding to those obtained in the experiment). After each break of the strain path at the points A, B, and C, in the strain diagram (see Fig. 4) one see reverse jumps of stresses [7], with the strain diagram becoming similar to the strain path for simple tension (dot-and-dashed curve).

Mozharovskii and Shukaev [8] performed an experimental study of the effect of strain path (uniaxial tension–compression and alternate torsion) on the fatigue life of 08Kh18N10T steel. In the experiments, the following parameters were varied:
the plastic strain rate amplitude

$$\Delta e_u^p = \sqrt{2/3}\sqrt{\Delta e_{ij}^p \Delta e_{ij}^p} = \sqrt{(\Delta e_{11}^p)^2 + (4/3)(\Delta e_{12}^p)^2}\,,$$

deformation mode angle

$$\psi = \arctan\,[(2/\sqrt{3}\,)\Delta e_{12}^p/\Delta e_{11}^p],$$

and phase shift angle θ between the axial strain and torsional strain amplitudes ($\theta = 0$ corresponds to proportional loading, and $\theta = 90^\circ$ to axial and shear strains, which vary in antiphase).

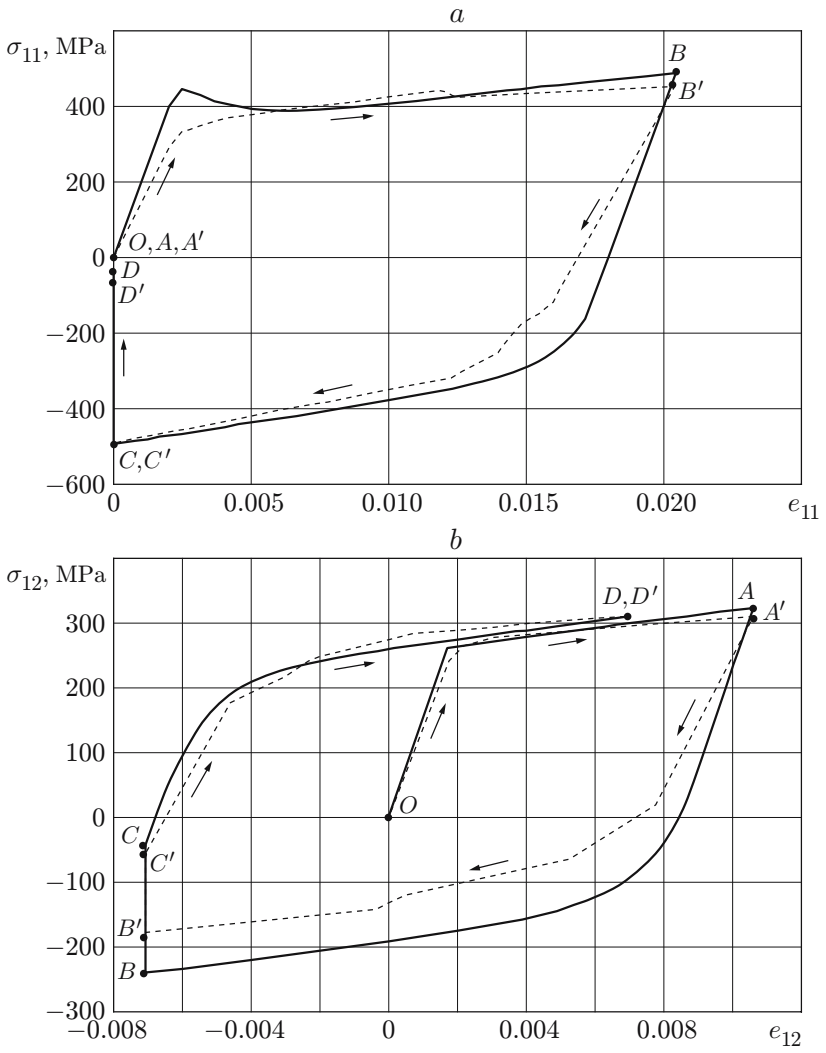

Fig. 3. Curves of $\sigma_{11}(e_{11})$ (a) and $\sigma_{12}(e_{12})$ (b): solid curves correspond to numerical results and dashed curve to experimental data [7].

The experimental results were processed to yield a regression equation between the number of cycles N_f before fatigue-crack formation and the plastic strain rate amplitude Δe_u^p (in percent), strain mode angle ψ (in degrees), and phase shift angle θ (in degrees):

$$\ln N_f = 10.5 - 7.5\Delta e_u^p + 1.71 \cdot 10^{-2}\psi - 6.367 \cdot 10^{-5}\psi^2 - 1.5839 \cdot 10^{-2}\theta$$

$$+ 8.41 \cdot 10^{-5}\theta^2 + 2.66 \cdot 10^{-2}\Delta e_u^p\,\theta + 3.133 \cdot 10^{-5}\psi^2\theta - 2.4 \cdot 10^{-3}\psi\theta + 1.372 \cdot 10^{-5}\psi\theta^2 - 2.04 \cdot 10^{-7}\psi^2\theta^2. \quad (19)$$

An analysis of the experimental data shows that the parameters ψ and θ have a significant effect on fatigue life.

Theoretical estimates of fatigue life for uniaxial tension–compression or alternate torsion obtained from experimental data using Coffin–Manson type equations and the equivalence criterion for the strain rate amplitude Δe_u^p may be erroneous. In the case of disproportionate loading at the same plastic strain rate amplitude, the fatigue life may be 4–6 times smaller than the strength for proportional loading (uniaxial tension–compression or alternate torsion).

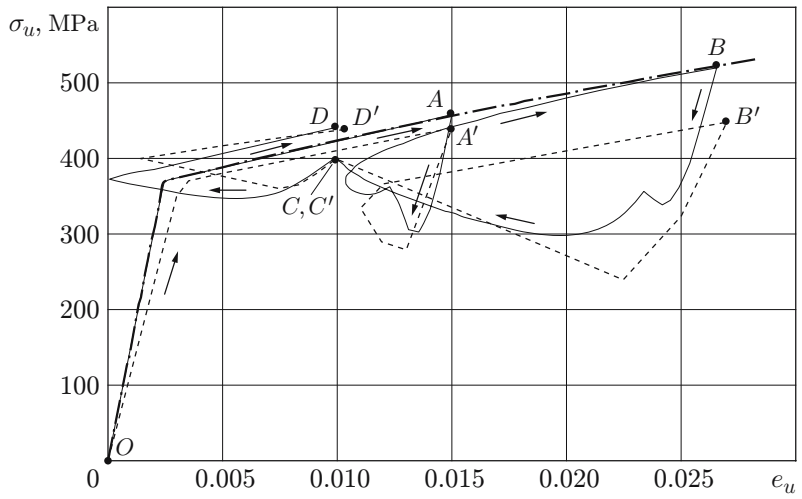

Fig. 4. Curves of $\sigma_u(e_u)$ for complex deformation of the material: the solid curve corresponds to numerical results and the dashed curve to experimental data [7]; the dot-and-dashed curve shows the strain path for uniaxial tension.

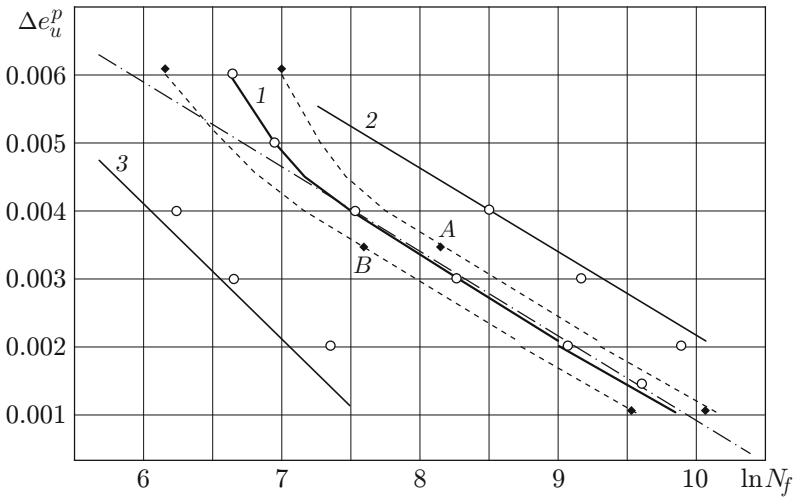

Fig. 5. Fatigue curves for 08Kh18N10T steel: solid curves correspond to experimental data [8], points to corresponding calculated data, and dashed curves to the scatter of experimental data about the averaged fatigue curve; 1) $\ln N_f = 10.5 - 7.5\,\Delta e_u^p$ (uniaxial tension–compression); 2) $\ln N_f = 11.523 - 7.5\,\Delta e_u^p$ [alternate torsion ($\psi = 90°$, $\theta = 0$)]; 3) simultaneous action uniaxial tensions–compression and alternate torsion.

Figure 5 shows experimental fatigue curves obtained according to the regression equation (19). For uniaxial tension–compression (curve 1), the fatigue life is described by the equation

$$\ln N_f = 10.5 - 7.5\Delta e_u^p$$

[the first two terms of Eq. (19)]. The dashed curves show the scatter of the experimental data about the averaged fatigue curve for 08Kh18N10T steel. It is evident that, at the plastic strain rate amplitude $\Delta e_u^p > 0.004$, relation (19) does not fit the experimental data. Curve 2 in Fig. 5 corresponds to alternate torsion:

$$\ln N_f = 11.523 - 7.5\Delta e_u^p$$

[$\psi = 90°$ and $\theta = 0$ in Eq. (19)]. Curve 3 corresponds to the fatigue life for simultaneous uniaxial tension–compression with amplitude Δe_{11}^p and alternate torsion with amplitude $\Delta e_{12}^p = (2/\sqrt{3})\Delta e_{11}^p$ and phase shift Δe_{11}^p, Δe_{12}^p on 90° (which corresponds to a square path).

TABLE 1

Monotonic Hardening Modulus q_χ at $T = 20°$C

χ_i	q_χ, MPa	χ_i	q_χ, MPa
0	−17000	0.015	1159
0.003	−4000	0.018	1117
0.006	1300	0.021	1107
0.009	1300	0.400	0
0.012	1185		

TABLE 2

Cyclic Hardening Modulus $Q_s(\rho_{\max})$ at $T = 20°$C

$\rho_{\max}$	Q_s, MPa	$\rho_{\max}$	Q_s, MPa
0	184	50	174
20	173	60	183
30	171	80	217
40	169	100	270

TABLE 3

Fracture Work $W_a(\rho_{\max})$ at $T = 20°$Cand $W_f^p = 3685$ MJ/m^3

$\rho_{\max}$, MPa	W_a, MJ/m^3	$\rho_{\max}$, MPa	W_a, MJ/m^3
0	1270	69	945
15	1270	72	492
30	1270	74	202
41	1270	76	66
51	1230	78	0
65	1046		

Equations (1)–(18) were used to calculate the elastoplastic strain and fatigue life of thin-walled tubular specimens made of 08Kh18N10T steel for various laws of variation of the axial strain e_{11} and torsional strain e_{12} at a temperature $T = 20°$C. The calculation results were compared with available experimental data. In the calculations, the following physicomechanical characteristics and model parameters were used: $K = 172{,}920$ MPa, $C_1 = 78{,}700$ MPa, $E = 205{,}000$ MPa, $\alpha = 0.0000166$ deg^{-1}, $C_p^0 = 184.5$ MPa, $g_1 = 23{,}236$ MPa, and $g_2 = 358.6$. The remaining parameters of the equations are given in Tables 1–3.

In Fig. 5, the points show the calculated fatigue life for the same amplitude Δe_u^p for three strain paths. The fracture work $W_f^p = 3685$ MJ/m^3 was determined using the point A in the fatigue curve 2.

Conclusions. A mathematical model of fracture mechanics was developed to describe complex plastic strain and damage accumulation in structural materials (metals and alloys under multiaxial disproportionate loading. The proposed model considers:

— the monotonic and cyclic hardening and cyclic memory effects of materials under proportional and disproportionate deformation, including cyclic transitions and stabilized cyclic behavior;

— the local anisotropy of plastic strain for break of strain paths.

The comparison of the calculated and experimental data (points and solid curves in Fig. 5, respectively) on the fatigue life of metals leads to the following conclusions:

— For known parameters of the constitutive relations for one experimental point (for example, the points A and B of curves 2 and 1), the low-cycle fatigue curve for uniaxial tension–compression or torsion is calculated with high accuracy for both large ($\Delta e_u^p = 0.006$) and small ($\Delta e_u^p = 0.001$) amplitudes of plastic strain intensities;

— The equations of fracture mechanics allow high-accuracy calculations of the low-cycle fatigue life of structural steels under disproportionate loading with variations of the axial e_{11} and shear e_{12} strains;

— The total- or plastic-strain rate and the plastic strain path length χ are not equivalence criteria for low-cycle fatigue processes and their use for the case of disproportionate loading leads to a considerable overestimation of the calculated strength over the real value;

— an equivalence criterion for fatigue processes is the energetic parameter y (y_e, y_p) of Eq. (14), which is the internal time of fatigue damage accumulation for various loading paths. In the case of regular processes for which it is possible to identify regular cycles, the parameter y is expressed in terms of the relative number of loading cycles: $y = N/N_f$, and Eq. (14) becomes

$$\omega = 1 - [1 - (N/N_f)^{\alpha+1}]^{1/(k+1)}.$$

For $\alpha = r = 0$, Eq. (14) leads to the well-known rule of linear summation of damage:

$$\omega = \sum \frac{N}{N_f}, \qquad \omega_f = 1.$$

Thus, Eqs. (1)–(18) describe inelastic deformation and fatigue damage accumulation before macrocrack formation in an elementary volume of a material under complex plastic deformation. The further fracture occurs primarily by growth of the macrocracks formed.

REFERENCES

1. F. M. Mitenkov, G. F. Gorodov, Yu. G. Korotkikh, et al. (eds.), *Methodology, Methods, and Means of Operational Monitoring of Transport Nuclear Power Plants* [in Russian], Mashinostroenie, Moscow (2006).
2. D. A. Kazakov, S. A. Kapustin, and Yu. G. Korotkikh, *Modeling of Deformation and Fracture of Materials and Structures* [in Russian], Nizhny Novgorod State University, Nizhny Novgorod (1999).
3. G. A. Makovkin, "Comparative analysis of disproportionality parameters of complex elastoplastic deformation," *Vest. Nizhegorod. Gos. Univ.*, No. 1, Nizhny Novgorod (1999), pp. 30–36.
4. Yu. G. Korotkikh, I. A. Volkov, and I. Yu. Gordleeva, "Modeling elastoplastic deformation of steels under complex loading," in: *Stability, Plasticity, and Creep under Complex Loading* (collected scientific papers) [in Russian], No. 2, Tver' State Tech. Univ., Tver' (2000), pp. 60–65.
5. V. G. Zubchaninov, N. L. Okhlopkov, and V. V. Garannikov, *Experimental Plasticity*, Book 1: *Complex Deformation* [in Russian], Tver' State Tech. Univ., Tver' (2003).
6. V. G. Zubchaninov, N. L. Okhlopkov, and V. V. Garannikov, *Experimental Plasticity*, Book 2: *Complex Deformation* [in Russian], Tver' State Tech. Univ., Tver' (2004).
7. V. G. Zubchaninov, V. I. Gulteev, and D. V. Zubchaninov, "Experimental study of complex loading of materials on multi-link paths," in: *Modern Problems of Thermoviscoplasticity*, Proc. 2nd Workshop, MAMI Moscow State Tech. Univ., Moscow (2007), pp. 19–24.
8. N. S. Mozharovskii and S. I. Shukaev, "Strength of structural materials under disproportionate low-cycle loading," *Probl. Prochnosti*, No. 10, 47–53 (1988).